Characterization of Ring-Bar and Contrawound Helix Circuits for High-Power Traveling-Wave Tubes

Daniel Teixeira Lopes and Cláudio C. Motta, *Member, IEEE*

***Abstract*—In this paper, we present results from an extensive study concerning the phase velocity and the interaction impedance characteristics of slow-wave structures (SWSs) for high-power traveling-wave tubes (TWTs). The SWS under analysis is the ring-bar one, which has been very suitable when high-power levels are needed in TWTs. We develop an analytical model based on the contrawound helix theory, which allows us to characterize the electromagnetic behavior of an equivalent ring-bar SWS. The theoretical model presented in this paper is able to reproduce all previously published results for the contrawound helix, and we also present new results. Additionally, we compare analytical results from the model to experimental results and to 3-D simulation results obtained using CST Microwave Studio.**

***Index Terms*—Contrawound helix, interaction impedance, phase velocity, power traveling-wave tube (TWT), ring bar, slow-wave structure (SWS).**

I. Introduction

SINCE THE invention of the traveling-wave tube (TWT) 60 years ago, many efforts have been made in order to obtain better mathematical models to aid in the design of more efficient devices. In recent years, numerical codes have become very attractive and powerful tools to simulate the electromagnetic behavior of microwave electron devices. On the other hand, analytical models are still useful for rapidly predicting slow-wave circuit characteristics over a wide array of circuit geometries.

For the design of high-power TWTs, which have extensive application in radar, satellite, and general defense systems, we develop in this paper a mathematical model to predict both the dispersion and interaction impedance characteristics for a contrawound helix [Fig. 1(a)] equivalent to an actual ring-bar slow-wave structure (SWS) shown in Fig. 1(b). The ring-bar SWS was first described by Birdsall and Everhart [1] as a practical construction form of the contrawound (also called cross-wound or twin tape) helix invented by Chodorow and Chu [2].

Although the single-tape helix behavior is well known and has motivated a large number of papers, there are few published papers about ring-bar and/or contrawound helices. We therefore present an extensive study of the propagation characteristics of the ring-bar and contrawound helices and compare it to that of single-tape helices.

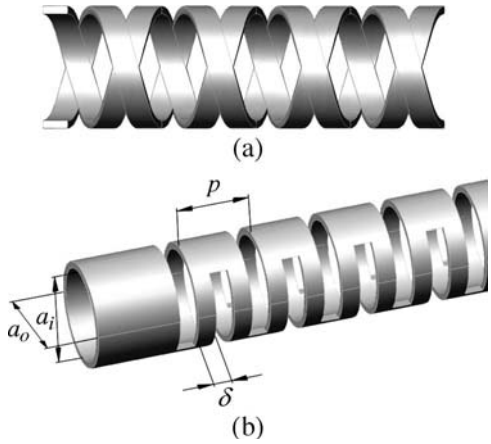

Fig. 1. (a) Contrawound helix and (b) ring-bar SWSs.

In order to describe the ring-bar structure, we use its equivalent contrawound helix model in an approach likewise presented by Cain and Grow [3]. They studied the effects of the dielectric and the metal loading on the dispersion characteristic of a contrawound helix. Our contribution is to show results not only for the dispersion characteristics but also for the interaction impedance and several comparative results between contrawound and single-tape helices. These results clearly show why contrawound helices are more suitable for high-power operational levels than single-tape helices. Additionally, we compare our contrawound helix theory with data measured from a ring-bar circuit and also with simulation results of the ring-bar circuit using the full 3-D eigensolver CST Microwave Studio.

II. Mathematical Model

In this section, we develop analytical expressions for the phase velocity and the interaction impedance characteristics of a contrawound helix.

A. Modeling the Actual SWS

A cross section of the actual structure under study is shown in Fig. 2(a), as well as its simplified model in Fig. 2(b). a_i is the helix inner radius, a_o is the helix outer radius, and b is the inner guide radius. The model was built using two concentric cylindrical regions. Region 1 is defined by $0 \leq \rho \leq a$, where $a = (a_i + a_o)/2$ is the actual ring-bar circuit mean radius. This region is considered as vacuum, with relative permittivity $\varepsilon_1 = 1$. The region is defined by $a \leq \rho \leq b$, for which we assume an

Manuscript received December 13, 2007; revised June 6, 2008. This work was supported in part by the State of São Paulo Research Foundation under Grant 05/03612-0 and by the National Council for Scientific and Technological Development. The review of this paper was arranged by Editor W. L. Menninger.

D. T. Lopes is with the Nuclear and Energetic Research Institute, University of São Paulo, São Paulo, SP 05508-000, Brazil (e-mail: danteixe@yahoo.com.br).

C. C. Motta is with the Brazilian Navy Technology Center, São Paulo, SP 05508-000, Brazil, and also with the University of São Paulo, São Paulo, SP 05508-000, Brazil (e-mail: ccmotta@usp.br).

Digital Object Identifier 10.1109/TED.2008.927804

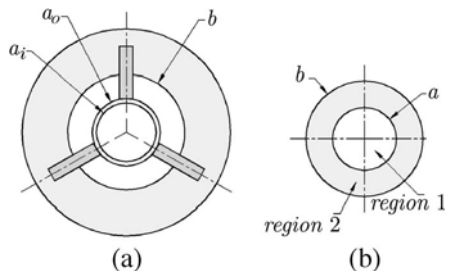

Fig. 2. (a) Cross section of the actual structure under study and (b) its simplified (in two regions) mathematical model.

effective relative permittivity due to the effect of dielectric support rods. This approach, known as region homogenization [4], simplifies the mathematical work at the cost of some accuracy.

B. Slow-Wave Solutions

The well-known general solution for Maxwell's equations applied to the propagation of slow-waves in a structure with cylindrical geometry is given by

$$\begin{matrix} E_{z,i} \\ H_{z,i} \end{matrix} = \sum_{l,m} A_{2(l,m)} \times \left[\begin{matrix} A_{i(l,m)} \\ C_{i(l,m)} \end{matrix} I_l\left(\gamma_{2(l,m)}\rho\right) + \begin{matrix} B_{i(l,m)} \\ D_{i(l,m)} \end{matrix} K_l\left(\gamma_{2(l,m)}\rho\right) \right] \times e^{jl\varphi} e^{-j\beta_{l,m}z} \tag{1}$$

where $E_{z,i}$ and $H_{z,i}$ are the electric and magnetic fields, respectively, for region i ($i = 1, 2$), i.e., solutions of the homogeneous scalar wave equation. A, B, C, and D are amplitude coefficients for the electric and the magnetic field components. I_l and K_l are the modified Bessel functions of first and second kind, respectively. γ_i is the radial propagation constant for the region i (γ_i is also the radial eigenvalue of the boundary value problem) defined as

$$\gamma_{i(l,m)} = \sqrt{\beta_{l,m}^2 - \varepsilon_i k_0^2} \tag{2}$$

where k_0 is the propagation constant in free space. The axial propagation constant in the SWS $\beta_{l,m}$ is given by

$$\beta_{l,m} = \beta_{0,0} + (l + 2m)\frac{2\pi}{p} \tag{3}$$

according to Floquet's theorem [5]. The double summation over two indexes (l, m) is used because of the symmetry properties of the contrawound helix, in order to ensure the correct field parity, so that fundamental TM field components from both helices add in phase whereas the corresponding TE field components add out of phase. Also, every undefined summation in l, m must be considered from $-\infty$ to ∞ unless other information is given. The other field components E_ρ, E_φ, H_ρ, and H_φ can be obtained by handling Maxwell's equations in the absence of source terms.

For the regions 1 and 2, boundary conditions cause two of the field amplitude coefficients in (1) to vanish. These boundary conditions are the field finiteness at $\rho = 0$ and the tangential electric and the normal magnetic field nullities at $\rho = b$, and thus, the field expressions for the regions 1 and 2 are

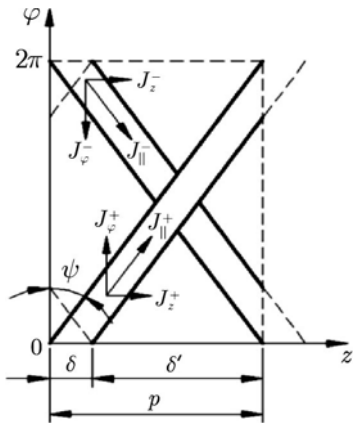

Fig. 3. Density current scheme assumed for a contrawound helix under the nontouching thin tape approximation.

$$E_{z,1} = \sum_{l,m} A_{1(l,m)} I_l\left(\gamma_{1(l,m)}\rho\right) e^{jl\varphi} e^{-j\beta_{l,m}z} \tag{4}$$

$$E_{z,2} = \sum_{l,m} A_{2(l,m)} \left[I_l\left(\gamma_{2(l,m)}\rho\right) - \frac{I_l\left(\gamma_{2(l,m)}b\right)}{K_l\left(\gamma_{2(l,m)}b\right)} K_l\left(\gamma_{2(l,m)}\rho\right) \right] \times e^{jl\varphi} e^{-j\beta_{l,m}z} \tag{5}$$

$$H_{z,1} = \sum_{l,m} C_{1(l,m)} I_l\left(\gamma_{1(l,m)}\rho\right) e^{jl\varphi} e^{-j\beta_{l,m}z} \tag{6}$$

$$E_{z,2} = \sum_{l,m} C_{2(l,m)} \left[I_l\left(\gamma_{2(l,m)}\rho\right) - \frac{I_l'\left(\gamma_{2(l,m)}b\right)}{K_l'\left(\gamma_{2(l,m)}b\right)} K_l\left(\gamma_{2(l,m)}\rho\right) \right] \times e^{jl\varphi} e^{-j\beta_{l,m}z} \tag{7}$$

where the prime indicates the differentiation of modified Bessel functions with respect to their arguments.

C. Boundary Conditions at the Helix Surface

We apply the boundary conditions from the contrawound helix model to obtain a group of four equations at the helix surface. These conditions are the following:

1) the continuity of the tangential components of the electric field between regions 1 and 2

$$E_{z,1}(\rho = a) = E_{z,2}(\rho = a) \tag{8}$$
$$E_{\varphi,1}(\rho = a) = E_{\varphi,2}(\rho = a) \tag{9}$$

2) the discontinuity of the magnetic field components equal to the current density over the helix surface

$$H_{z,1}(\rho = a) - H_{z,2}(\rho = a) = J_\varphi \tag{10}$$
$$H_{\varphi,2}(\rho = a) - H_{\varphi,2}(\rho = a) = J_z \tag{11}$$

where $J_\varphi (= J_\varphi^+ + J_\varphi^-)$ is composed by the current densities that flow in the helix tapes wound in opposite directions as shown in Fig. 3.

The same statement is valid for $J_z(=J_z^+ + J_z^-)$, the axial component of the current densities that flow in the helix tapes wound in opposite directions. Fig. 3 shows a planar view for the contrawound helix and its assumed current scheme. The plus superscript is used for the left-handed helix, and the minus superscript is used for the right-handed helix. One should note that the azimuthal current densities have opposite directions whereas axial components have the same directions. This is the kernel of the symmetric mode of propagation supported by the contrawound helix and, likewise, by the ring-bar circuit. Although similar, the ring-bar circuit is not identical to the contrawound helix, and some distortion in the field pattern is obviously expected; however, experience suggests that the field patterns are similar.

Assuming the thin tape approximation, the current densities are decomposed as

$$J_z^+ = J_\parallel^+ \sin\psi \tag{12}$$

$$J_z^- = J_\parallel^- \sin\psi \tag{13}$$

$$J_\varphi^+ = -J_\parallel^+ \cos\psi \tag{14}$$

$$J_\varphi^- = J_\parallel^- \cos\psi \tag{15}$$

where $J_\parallel$ is the current density parallel to the helix tapes. The plus and the minus superscripts indicate the left-handed and the right-handed tapes, respectively, as before.

The symmetry properties of the contrawound helix allow $J_\parallel^-$ to be expressed as $J_\parallel^+$ using its Fourier series, which can be represented as

$$\sum_{l,m} J_{\parallel(l,m)}^- e^{jl\varphi} e^{-j\beta_{l,m}z} = \sum_{l,m} J_{\parallel(l,m)}^+ e^{-jl\varphi} e^{-j\beta_{l,m}z} \tag{16}$$

where $J_{\parallel(l,m)}^-$ and $J_{\parallel(l,m)}^+$ are the corresponding coefficients of the series.

D. Dispersion Equation

In order to obtain a dispersion equation, we followed the guidelines given by Chodorow and Chu [2] and also presented by Cain and Grow in the appendix of [3]. These consist of using a variational technique. In this case, the suitable function to be varied is the Lagrangian for the electromagnetic field, which becomes

$$L = jk_0 a Z_0 \int_0^p \int_0^{2\pi} \left[E_\varphi^*(\rho=a)J_\varphi + E_z^*(\rho=a)J_z\right] d\varphi dz \tag{17}$$

where Z_0 is free space impedance and the asterisk indicates the complex conjugate of the quantity. The exact solution requires $\delta L = 0$, but we approximate the solution by setting $L = 0$. We use the one-term approximation for the current density, which is known to yield reliable results [2], [3], [6].

E. Interaction Impedance

Once one has solved the dispersion equation and found suitable propagation constants for given frequencies, the interaction impedance on the axis of the SWS can be obtained by using Pierce's formula [7], which can be written in a generalized form

$$\mathcal{K}_l(\omega,\rho) = \frac{\left|E_{z(l,0)}(\omega,\rho)\right|^2}{2\beta_{l,0}^2(\omega)P_T(\omega)} \tag{18}$$

where $P_T(\omega)$ is the total electromagnetic power propagated in the SWS and can be found in the usual way from Poynting's complex theorem. Thus, the total power propagated in the SWS is

$$P_T = \frac{1}{2}\mathrm{Re}\int_0^{2\pi}\int_0^b \left[E_\rho H_\varphi^* - E_\varphi H_\rho^*\right] \rho d\rho d\varphi. \tag{19}$$

The complete expression for P_T is quite large, but can be found in full detail in [8]. The Pierce impedance (or zero-order) formula is obtained when $\rho = 0$ and $l = 0$. We considered ± 5 space harmonics in calculations.

Some consideration must be made in order to calculate the interaction impedance of higher order harmonics, as the backward wave, for example, because nonfundamental electric field components vanish at the axis. We prefer to calculate the interaction impedance for the backward mode at the radial coordinate correspondent to the edge of the electron beam. We consider that it is a kind of worst-case calculation. Let us call ρ_e the radial coordinate of the beam's edge. For $\rho > \rho_e$, there are no longer electrons to interact with the backward wave even though its interaction impedance increases as ρ increases up to helix radius (where there is no tape). For $\rho < \rho_e$, the interaction impedance for the backward mode decreases and decays to zero at the axis. Concluding, the edge of the beam is the radial coordinate of greater interaction impedance where electrons can effectively interact with the backward wave.

F. Simulations Using CST Microwave Studio Eigensolver

In order to compare the results of the analytic expressions to ones from a commercial full 3-D eigensolver, we used the CST Microwave Studio [9] to simulate one period of a ring-bar structure used in an experimental work. The single-period simulation method has been shown to work quite well when used with periodic boundary conditions [10], [11]. The modeled domain is shown in Fig. 4. The region between the ring-bar circuit and the circular shield guide can be set with either vacuum properties or another dielectric material. The solution converges with approximately 200 000 mesh cells. All metallic parts were set as perfect electric conductor, and the dielectric in region 2 was set nondispersive with a permittivity of 2.6 in the loaded case.

III. Results and Discussion

We present first results obtained from the theoretical model developed in Section II and then comparisons with simulated

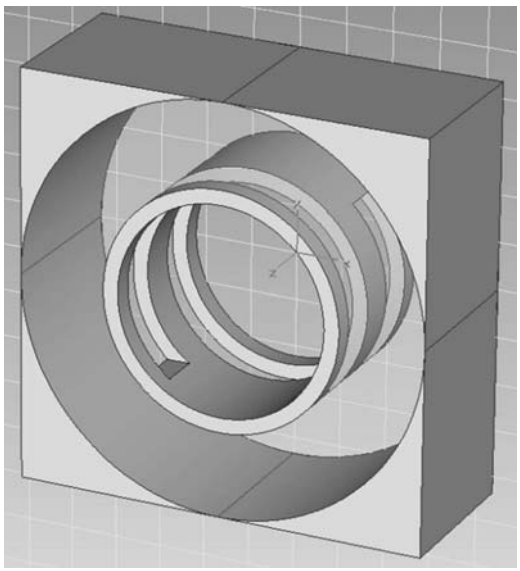

Fig. 4. Illustration of the domain generated using CST Microwave Studio to simulate a ring-bar circuit.

results from the 3-D eigensolver software and with experimental results [8].

A. Effect of the SWS Parameters

It is known that the helix period p (or the helix pitch angle ψ) is a critical parameter affecting the helix phase velocity. We analyzed this effect varying the parameter $\cot\psi(=2\pi a/p)$ and plotting curves for the phase velocity and the interaction impedance as a function of the normalized wavenumber k_0a. Fig. 5(a) shows that the phase velocity decreases as the helix period decreases in relation to the helix radius. Additionally, the upper cutoff frequency is increased as $\cot\psi$ is increased. The interaction impedance shown in Fig. 5(b) has more complicated behavior because it increases for $k_0a < 0.4$ and decreases for $k_0a > 0.4$ as $\cot\psi$ is increased.

The effect of the tape width on the phase velocity and the interaction impedance is shown in Fig. 6. As before, phase velocity and interaction impedance are plotted as a function of the normalized wavenumber. The variation parameter is the tape width-to-period ratio $\eta=2\pi\delta/p$. Fig. 6(a) shows that the phase velocity decreases as the tape width decreases until the tape becomes an infinitesimal wire. The cutoff frequency also decreases as the tape width is decreased. As before, the interaction impedance behavior [Fig. 6(b)] is more complicated. For low values of k_0a, the interaction impedance increases as the tape width is decreased. However, for higher values of k_0a, the interaction impedance decreases if the tape width is increased.

The effect of the shield guide inner radius is shown in Fig. 7, which shows plots of the phase velocity (a) and the interaction impedance (b) as a function of the normalized wavenumber and the ratio $r = b/a$. It is shown that, if the shield guide is closer to the helix (lower values of r), the SWS becomes a very broad band structure, as expected based on the common technique of using vanes near the helix for increasing helix circuit bandwidth. The interaction impedance is correspondingly reduced for lower values of r.

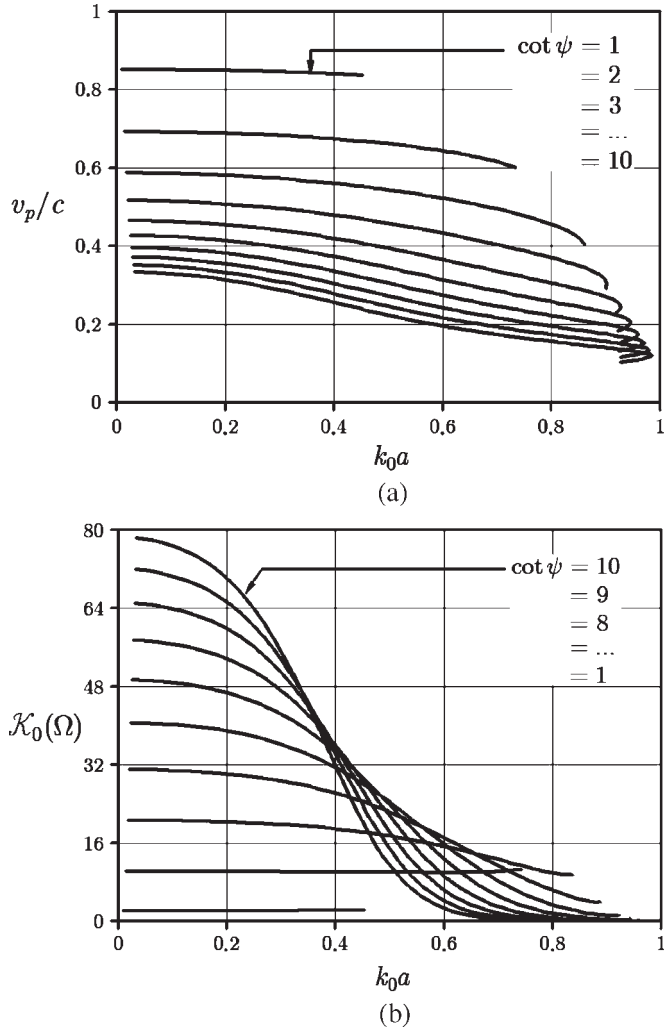

Fig. 5. (a) Phase velocity and (b) interaction impedance as a function of the frequency and the helix pitch to radius ratio $\cot\psi = 2\pi a/p$.

The effect of varying the effective relative permittivity of region 2 (ε_2) is shown in Fig. 8. Because this quantity is proportional to the number of support rods, their cross-sectional area, and their permittivity, one can verify the influence of increasing or decreasing one of these parameters. Fig. 8 shows that increasing ε_2 decreases both the phase velocity (a) and the interaction impedance (b). Additionally, the cutoff frequency is also decreased and the dispersion envelope remains nearly the same.

B. Comparison Between Single-Tape Helix and Contrawound Tape Helix

Chodorow and Chu [2] reported that the contrawound helix is more dispersive and presents about twice the interaction impedance of a single-tape helix with the same phase velocity. To verify these statements, we plotted the phase velocity and the interaction impedance for both the single-tape and the contrawound helix in two situations. Fig. 9 shows the result when both SWSs have the same geometrical parameters, and Fig. 10 shows the results when both SWSs are adjusted to present the same phase velocity at a frequency near 8 GHz ($k_0a/\cot\psi \approx 0.03$).

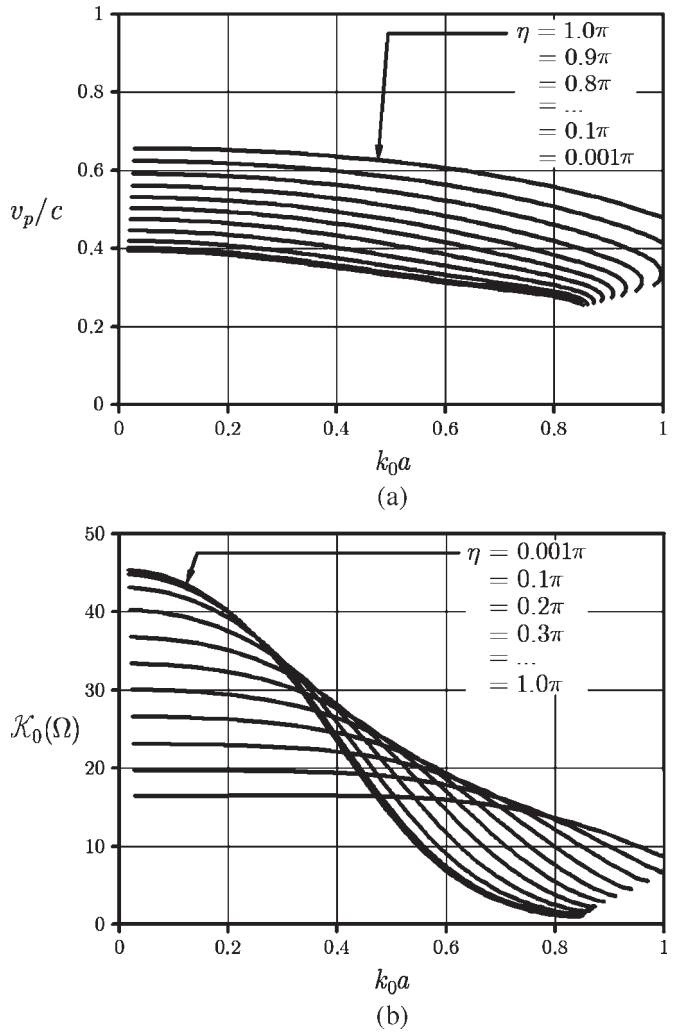

Fig. 6. (a) Phase velocity and (b) interaction impedance as a function of the frequency and the tape width to helix period ratio $\eta = 2\pi\delta/p$.

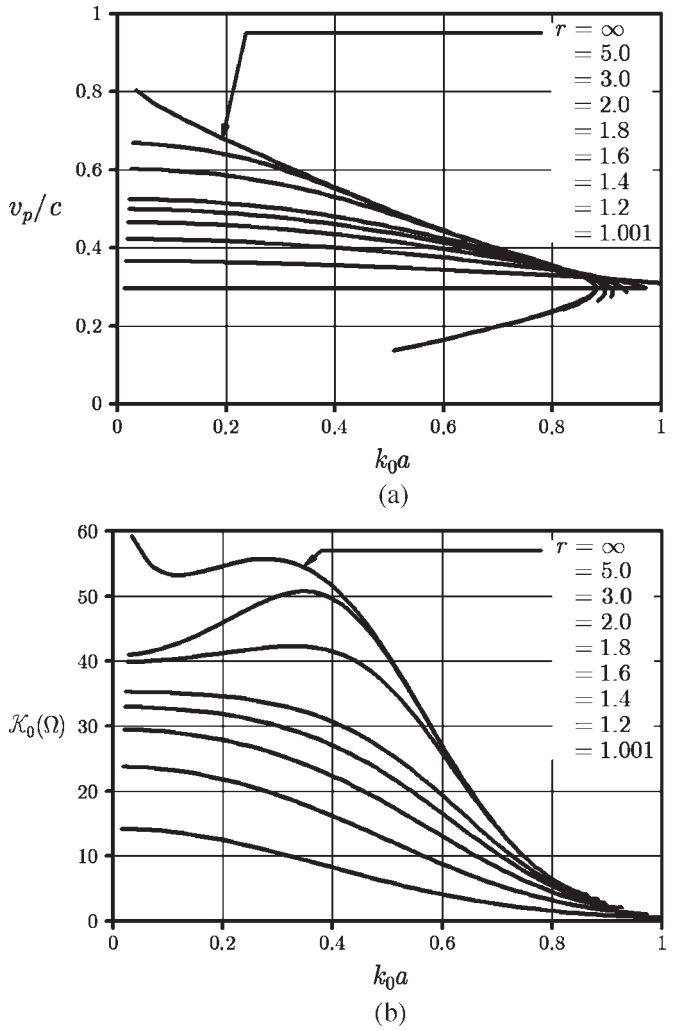

Fig. 7. (a) Phase velocity and (b) interaction impedance as a function of the frequency and the guide-to-helix radius ratio $r = b/a$.

One can see in Fig. 9 that, for the same geometry, the contrawound helix has about twice the phase velocity of the single-tape helix. The contrawound helix is, as expected, more dispersive than single-tape helix and, additionally, has a higher cutoff frequency. It is also shown that only at low frequencies, or for cases where the number of turns per wavelength is greater than $\sim$4, is the interaction impedance higher for the single-tape helix. However, when two SWSs have different phase velocities, we cannot compare them satisfactorily. Fig. 10 therefore shows the phase velocity (a) and the interaction impedance (b) characteristics for single-tape and contrawound helices that are adjusted to present the same phase velocity near $k_0a/\cot\psi \approx 0.03$ (or $\sim$9 periods per wavelength). Fig. 10 clearly demonstrates the higher dispersion and interaction impedance of the contrawound helix circuit. Interestingly, at the point where the two SWSs have the same phase velocity, the ratio of the contrawound helix impedance to the single-tape helix impedance peaks at approximately 2.3.

C. Experimental Results From a Ring-Bar SWS

We now show measurements of the phase velocity and the interaction impedance performed on a ring-bar structure with $a = 2.375$ mm, $r = 1.831$, $\cot\psi = 4.239$, $\eta = 1.571$, and $\varepsilon_2 = 1.85$. The objective is to verify how much the theoretical model developed from the contrawound helix agrees with ring-bar experimental data. The measurement setup and techniques are based on the nonresonant perturbation methods and are described in detail in [8].

Measurement data for phase velocity are shown in Fig. 11(a). Curves indicated by $\varepsilon_2 = 1.0$ refer to the absence of support rods, i.e., the effective relative permittivity of the region 2 is equal to that of the region 1 (vacuum). Curves indicated by $\varepsilon_2 = 2.6$ refer to the SWS loaded by a lucite pipe inserted between the helix and the shield guide wall (region 2). The phase velocity measured on the ring-bar SWS is smaller than that predicted for the contrawound helix and is also more dispersive. As the frequency increases, the discrepancy increases from 4% at 7 GHz to about 40% at 12 GHz. This result is expected in light of some data presented in [1], which indicate that the ring-bar circuit is more dispersive than contrawound circuit. However, the amount of phase velocity reduction due to the dielectric loading is predicted with satisfactory accuracy. Theoretically, the phase velocity is reduced by about 63% when the SWS is loaded as mentioned before. The experimental result points to a value about 61%.

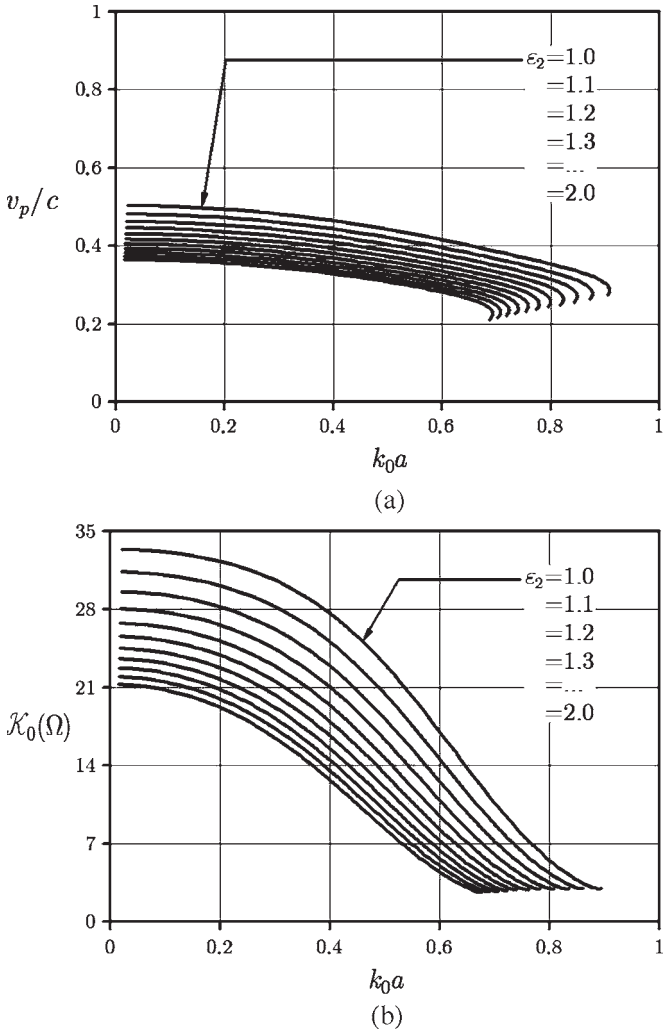

Fig. 8. (a) Phase velocity and (b) interaction impedance as a function of the normalized wavenumber and the effective relative permittivity of region 2 ε_2.

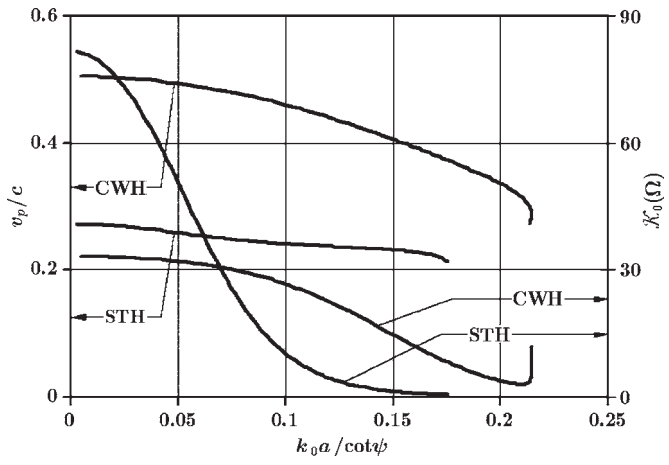

Fig. 9. Phase velocity and interaction impedance as a function of the normalized wavenumber for (STH) single-tape and (CWH) contrawound helices with the same geometric parameters.

The interaction impedance measured on the ring-bar SWS is also more dispersive than that predicted for its equivalent contrawound helix. At frequencies below 10.5 GHz, measured

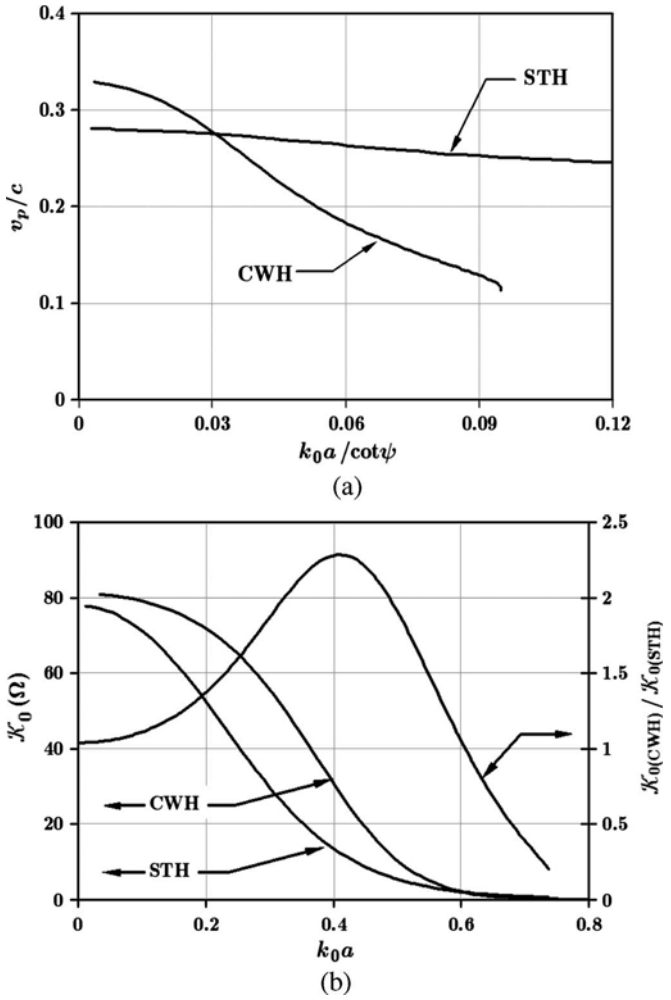

Fig. 10. (a) Phase velocity and (b) interaction impedance as a function of the normalized wavenumber for single-tape and contrawound helices with the same phase velocity at near (a) $k_0a/\cot\psi \gg 0.03$ and (b) $k_0a \gg 0.4$.

values are greater than predicted ones. Above this frequency, predicted values are greater. Experimental data shown in Fig. 11(b) are for the unloaded SWS.

CST Microwave Studio simulation results are shown to agree more satisfactorily with experimental data than with the analytical theory. The simulated phase velocity discrepancy is about 4% over the whole frequency range in the unloaded case. In the loaded case, the discrepancy is about 1% over the whole frequency range. The simulated result for the interaction impedance results shows a greater discrepancy than the phase velocity results. Relative to simulated values, measured values are ∼5% lower at around 8 GHz, up to 16% lower between 10 and 11 GHz, and ∼5% lower at 12 GHz. Simulations accounting for losses, using perturbation techniques and the frequency domain module of CST Microwave Studio, are planned in order to try to improve the simulation results.

Whereas there is clearly some discrepancy between our analytical theory and the measured (and 3-D simulation) results, we feel that the theory provides a valuable tool for quickly comparing different ring-bar or contrawound helix geometries and also for evaluating them against single-tape helix designs. The theory can further be calibrated to existing measured data to provide more confidence.

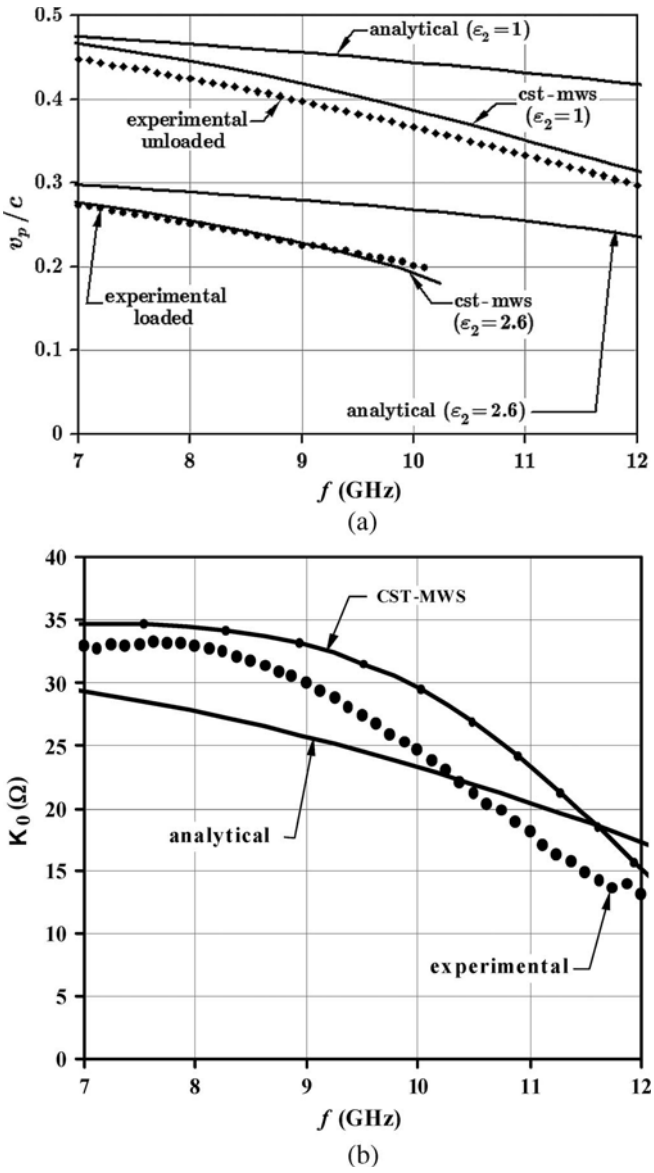

Fig. 11. (a) Experimental phase velocity and (b) interaction impedance as a function of the frequency.

IV. Conclusion

In this paper, we presented several results concerning the phase velocity and the interaction impedance characteristics of ring-bar and contrawound helix circuits used in high-power TWTs. A mathematical model was developed based on the contrawound helix. The theory enables rapid computation of ring-bar or contrawound circuit characteristics for comparison to single-tape helix circuits. Analytical results presented effectively show why contrawound helices are suitable for high-power operation levels in TWTs compared to single-tape helices. We compared our analytical model based on the contrawound helix with ring-bar experimental and 3-D eigensolver results.

Acknowledgment

The authors would like to thank the reviewers and the editor, Dr. W. L. Menninger, for the fruitful suggestions.

References

[1] C. K. Birdsall and T. E. Everhart, "Modified contra-wound helix circuits for high-power traveling-wave tubes," *IRE Trans. Electron Devices*, vol. 3, no. 4, pp. 190–204, Oct. 1956.
[2] M. Chodorow and E. L. Chu, "Cross-wound twin helices for traveling-wave tubes," *J. Appl. Phys.*, vol. 26, no. 1, pp. 33–43, Jan. 1955.
[3] W. N. Cain and R. W. Grow, "The effects of dielectric and metal loading on the dispersion characteristics for contrawound helix circuits used in high-power traveling-wave tubes," *IEEE Trans. Electron Devices*, vol. 37, no. 6, pp. 1566–1578, Jun. 1990.
[4] B. N. Basu, *Electromagnetic Theory and Applications in Beam-Wave Electronics*. Singapore: World Scientific, 1996.
[5] D. A. Watkins, *Topics in Electromagnetic Theory*. New York: Wiley, 1958.
[6] S. Sensiper, "Electromagnetic wave propagation on helical structures," *Proc. IRE*, vol. 43, no. 2, pp. 149–161, Feb. 1955.
[7] J. R. Pierce, *Traveling-Wave Tubes*. New York: Van Nostrand, 1950.
[8] D. T. Lopes, "Caracterização de estruturas de ondas lentas helicoidais para utilização em TWT de potência," "M.S. thesis," Instituto de Pesquisas Energéticas e Nucleares, Univ. São Paulo, São Paulo, Brazil, 2007.
[9] *CST Microwave Studio, User Manual*, Computer Simulation Technology GmbH, Darmstad, Germany, 2008.
[10] C. T. Chevalier, C. L. Kory, J. D. Wilson, E. G. Wintucky, and J. A. Dayton, Jr., "Traveling-wave tube cold-test circuit optimization using CST MICROWAVE STUDIO," *IEEE Trans. Electron Devices*, vol. 50, no. 10, pp. 2179–2180, Oct. 2003.
[11] M. Aloisio and G. Sorbello, "One-third-of-pitch reduction technique for the analysis of ternary azimuthally periodic helical slow-wave structures," *IEEE Trans. Electron Devices*, vol. 53, no. 6, pp. 1467–1473, Jun. 2006.

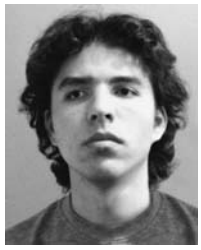

Daniel Teixeira Lopes was born in São Paulo, SP, Brazil, in 1981. He received the B.S. degree in materials, processes, and electronic components (with honors) from the Faculdade de Tecnologia de São Paulo in 2005 and the M.S. degree in nuclear technology from the Nuclear and Energetic Research Institute, University of São Paulo, São Paulo, in 2007, where he is currently working toward the Ph.D. degree.

In 2003, he was with the Brazilian Navy Technology Center, São Paulo, in a scientific initiation program. His research interest is slow-wave structure design for high-power traveling-wave tubes.

Cláudio C. Motta (M'97) received the B.S. degree in electrical engineering from the College of Engineering, São José dos Campos, SP, Brazil, the M.S. degree in plasma physics from the Technology Institute of Aeronautics, São José dos Campos, and the Ph.D. degree in laser-plasma physics from the University of São Paulo (USP), São Paulo, in 1982, 1986, and 1996, respectively.

Since 1987, he has been involved in the design and construction of power microwave tubes with the Brazilian Navy Technology Center, São Paulo, and since 2002, he has been an Associate Professor with USP. His research interests include microwave electronics and laser-plasma technology.

Dr. Motta is a member of the Microwave and Optoelectronics Brazilian Society.